IMPACT ENERGY ABSORPTION ABILITY OF THERMOPLASTIC POLYURETHANE (TPU) CELLULAR STRUCTURES FABRICATED VIA POWDER BED FUSION

Y. Wu*, J. Hermes†, L. Verbelen††, and L. Yang*

*Department of Industrial Engineering, University of Louisville, Louisville, KY 40292
†Department of Mechanical Engineering, University of Louisville, Louisville, KY 40292
††BASF 3D Printing Solutions, Heidelberg, Germany

Abstract

In this study, experimental based investigation was carried out with various cellular structure designs realized using a developmental thermoplastic polyurethane (TPU) fabricated by powder bed fusion process, in the attempt to evaluate the effectiveness of impact energy absorption design with cellular structures when combined with favorable materials. Various cellular designs including the re-entrant auxetic, double-arrow auxetic, octet-truss, BCC, octahedral, diamond and double bow-tie were designed and evaluated. Pendulum-rebound resilience testing and drop-weight impact testing were carried out with each designs, and the effective energy absorption capabilities of these designs were compared. The results from this study provide some initial insights into the design of TPU-based cellular structures for energy absorption applications that could benefit the establishment of more comprehensive knowledge base in this area.

Introduction

One of the technically important application areas of the cellular structures is the energy absorption applications, in which the cellular structures typically act as structural buffers and absorb energy via elastic and plastic deformation, and even fracture. Considering that in many of the energy absorption applications the energy incidents occur as energy spikes, such as the small object impact on an aircraft structures, or the collision and drop impact on a small hand-held equipment, the dynamic energy absorption characteristics of the cellular structures should be the focus of performance designs and evaluations. Typically the dynamic energy absorption event is characterized by the high strain rate of deformation of the structures resulted from either large force or acceleration/deceleration. Due to the increased significance of factors such as inertia force, strain rate sensitivity and adiabatic heating [1], the dynamic responses of the cellular structures could be significantly different from their quasi-static and low-strain rate characteristics. There exist an extensive amount of literature that investigate different aspects of the dynamic energy absorption of cellular structures. Traditionally, stochastic cellular structures, often referred to as foams, of different manufacturing technologies and base materials have been investigated for their energy absorption behaviors under various dynamic compressive strain rates [2-8]. These structures typically exhibit distinct three-stage compressive stress-strain characteristics, including the initial elastic stage, the plateau stage where the average stress levels of the structures vary relatively little as the strain accumulates, and the final densification stage, where the structures are compressive sufficiently and begin to behave like solid materials [9, 10]. Under higher strain-rate dynamic compression, the stochastic cellular structures often exhibit significantly increased

plateau stress levels, which is attributed to various factors such as entrapped gas/fluid phase [11], the microstructural characteristics [11, 12], and intrinsic material strain rate sensitivity [11]. On the other hand, due to the general lack of control of the microscopic cellular topology, the dynamic characteristics of the stochastic cellular structures are primarily dominated by the specific manufacturing process and the relative densities.

Introducing cellular topology design has been considered as a promising approach to overcome the limitation of the designability of the stochastic cellular structures. Various literatures have explored the dynamic energy absorption characteristics of various cellular topology designs [13-19]. Compared to the stochastic cellular structures, the local topology-induced effects, such as microinertia, stress concentration and heterogeneous deformation mode becomes much more significant in the dynamic characteristics with the non-stochastic cellular designs. For examples, Lee et al. investigated the dynamic and ballistic impact responses of a 304 stainless steel pyramidal truss structure, and noted that the local microinertia kinetic effect of the strut members, as well as the intrinsic material strain rate hardening play dominant roles in the early failure stage of the structures and the total energy absorption [15]. Numerous works have suggested that auxetic designs with negative Poisson's ratios exhibit significantly higher energy absorption capabilities compared to the regular cellular structures [13, 14]. Harris et al. investigated multiple 316L stainless steel cellular-thin wall hybrid cellular structures fabricated by laser powder bed fusion additive manufacturing (PBF-AM), and suggested that the hybrid designs exhibit the most significant energy absorption design potentials in the intermedium strain rate ranges where the dynamic local buckling effect is dominant [19]. Xiao et al. studied the dynamic energy absorption of Ti6Al4V rhombic dodecahedron cellular structures fabricated by electron beam PBF-AM, and noted the feasibility of unit cell-size based impact energy absorption design [17]. In the design of the energy absorption cellular structures, the multi-functionality requirements often require highly controlled cellular topology designs that are infeasible to most traditional manufacturing processes, which necessitates the use of additive manufacturing (AM) for design realization. Extensive amount of literature have demonstrated AM cellular structures for impact energy-absorbing purpose, and the results and discussions clearly suggested the importance of considering both the cellular geometry and the material properties [17-19].

Thermoplastic polyurethane (TPU) is a class of material that is utilized broadly for the manufacturing of stochastic cellular structures for energy absorption [20], and is a potentially promising material for AM energy absorption structure realization. Cellular TPU structures fabricated via material extrusion have been explored for their various mechanical properties including energy absorption, strain rate sensitivity and quasi-static mechanical strength [21-23]. In comparison, works that based on powder bed fusion AM (PBF-AM) are limited, which might be partly due to the immaturity of the powder-based AM TPU feedstock. On the other hand, due to the use of preheating and the powder feedstock, PBF-AM tends to exhibit higher geometry flexibility compared to the material extrusion based AM, which is potentially advantageous for the design of multi-objective energy absorption structures. One of such application areas is the sports helmet, which requires not only energy absorption capabilities, but also other performance criteria such as breathability, rigidity and shock buffering. Much additional works are needed to systematically understand the correlations between the cellular geometry design, the material properties and the energy absorption characteristics of TPU cellular structures fabricated via PBF-AM. Therefore, in the current work, experimental based investigation was carried out with TPU cellular structures of various cellular designs fabricated via a laser BPBF-AM process. The results were compared to each other in order to identify potential interactions between geometry and

materials, in the attempt to provide preliminary design selection guidelines for TPU cellular structures.

Cellular Design and Sample Preparation

As in theory there exist unlimited possibilities of cellular geometry designs, it is infeasible to exhaust the design variations. Therefore, a perhaps more feasible to investigate a small subset of cellular designs that represent a variety of different design scenarios. However, there are currently limited literature about the guidance of the cellular design scenarios. A few of the general design rules for the cellular structures that have been discussed include the primary structural deformation mode, which is determined via Maxwell stability criterion [24, 25], the Poisson's ratio of the structure [26, 27], the directional isotropy [28-30], and the presence of local strut buckling [31]. For example, generally a stretch-dominated cellular structures that have Maxwell stability criterion value $M \geq 0$ tend to exhibit higher elastic modulus and initial yield strength compared to the bending-dominated cellular structures ($M < 0$) at the same relative density levels [24]. Auxetic cellular structures with negative Poison's ratios exhibit some unusual characteristics compared to the ones with regular positive Poisson's ratios, such as high shear modulus, high indentation resistance, and high energy absorption [32-34]. In addition, directional anisotropy of cellular structures have been considered to establish the elastic performance bounds for the designs [29, 30]. Finally, the presence of buckling deformation failure mode within the cellular structure implies potentially catastrophic local failure [31]. Inspired by these design rules, various cellular geometries were designed and investigated in this study. 7 different types of cellular structures were designed, as listed in Table 1, which include the re-entrant auxetic (RA) and the double-arrow auxetic (DA) structures that exhibit negative Poisson's ratios but different presence of local buckling mode, the octet-truss (OT) and octahedral (OCT) structures that exhibit stretch-dominated deformation but different directional anisotropy, the BCC, diamond (D) and double bow-tie (DB) structures that exhibit bending dominated deformation but different direction anisotropy and presence of local buckling mode. Table 1 also lists the geometry design parameters for the cellular structures, with the corresponding variable designation shown in Fig.1. Considering the fact that relative density exerts dominant effects on the overall properties of cellular structures, for each cellular topology design, it was originally intended that 2 levels of relative densities were designed, which was realized by scaling the lengths of the struts while keeping the strut cross sectional dimension consistent (1mm). However, due to the thickness of the struts, the high density design variations for both the D and DB structures were not physically feasible and were therefore excluded from further investigation. In addition, it was later found that the high density design variation of the DA structure (DA2) resulted in un-cleanable samples, therefore the DA2 was also excluded from the experimental impact studies.

Two levels of relative densities, 0.15 and 0.25, were selected arbitrarily for the study. For each type of cellular topologies, the strut length and strut angles θ (when available) were also arbitrarily selected in that these geometry parameters might not result in the optimal impact energy absorption performance of that type of cellular topology. The resulting design variations exhibit relative densities within 10% of the intended values, which were expected to be insignificant for the intended comparisons.

Design	Type	L_1/H (mm)	L_2 (mm)	L_3 (mm)	θ (Deg)	t (mm)	RD

RA1	Re-entrant auxetic	4.3	5.344		75	1	0.156
RA2	Re-entrant auxetic	3.5	3.807		75	1	0.243
DA1	Double-arrow auxetic	8.5	5.45		75	1	0.140
DA2	Double-arrow auxetic	7	5.4		75	1	0.243
OT1	Octet-truss	7.3				1	0.147
OT2	Octet-truss	5.2				1	0.250
OCT1	Octahedral	6				1	0.152
OCT2	Octahedral	4.5				1	0.243
D1	Diamond	5.4			120	2	0.166
DB1	Double bow-tie	7.5			75	1	0.111
BCC1	BCC	8.2	8.2		125	1	0.145
BCC2	BCC	6	6		128	1	0.264

Table 1 Cellular structure design variations

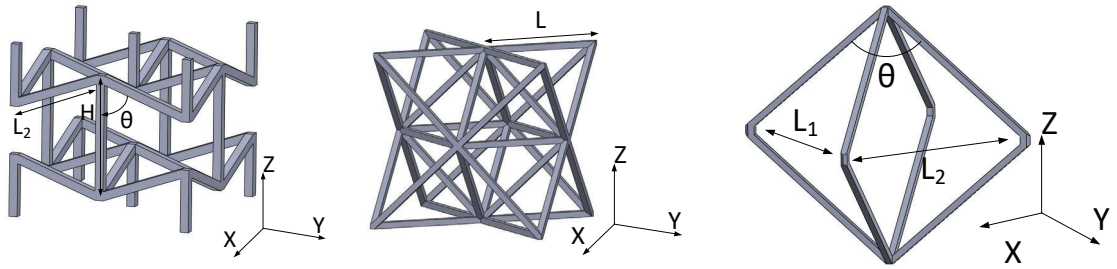

a. Re-entrant auxetic (RA) b. Octet-truss (OT) c. BCC

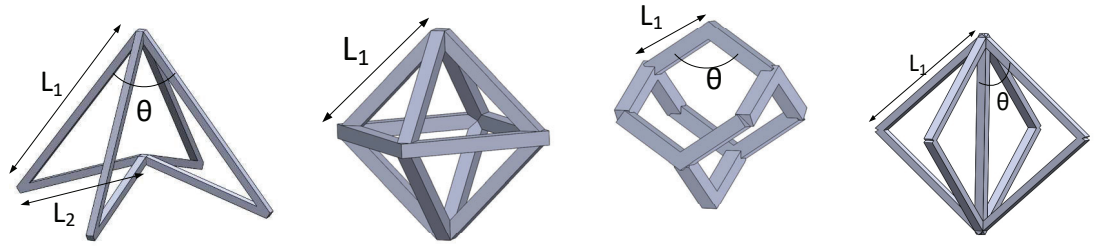

d. Double arrow (DA) e. Octahedral (OCT) f. Diamond (D) g. Double bow-tie (DB)

Fig.1 Unit cell designs and design parameters

The cellular unit cell designs were modeled in SolidWorks, then patterned orthogonally into a cylindrical volume using Materialise Magics. The overall geometry of the sample is shown in Fig.2a. The cylindrical sandwich panel skins have thickness of 1mm and diameter of 48mm, and the overall height is 15mm. Therefore, the overall dimensions of the cellular core are Φ48mmx13mm. The design geometry parameters were determined based on the DIN53512 standard for pendulum rebound testing. The samples were fabricated by an EOS P800 system using a developmental thermoplastic polyurethane (TPU) material at BASF 3D Printing Solutions headquarter, Heidelberg, Germany. The fabricated samples were cleaned using the typical

compressed air blowing method for laser sintering powder bed fusion parts. Some of the fabricated samples are shown in Fig.2b. Multiple samples (4-5) of each design variation were fabricated, which were intended for various types of mechanical testing. The samples were each measured by digital scope and caliper for weight and dimensional information. The relative densities of each samples were consequently calculated based on the reference solid material density value of 1g/cm^3 provided by the company. The dimensions and weights of each types of samples are shown in Table 2. In general, all the fabricated samples exhibit generally good dimensional accuracy and consistency, but significantly higher relative densities compared to the designed ones as shown in Table 1. This is largely attributed by the significant surface sintering that occurred on the surfaces of the cellular struts in the sandwich cores, as well as the incomplete post-fabrication cleaning, which could be noticed obviously as loose powder kept falling off from the samples during the experimental studies. Although due to the proprietary nature of the developmental material no specific process parameters were disclosed, it is expected that such excessive surface partial sintering effect is introduced by the high preheating temperature.

a. Sandwich design b. Typical samples

Fig.2 Sandwich structure sample designs

Design	Diameter (mm)	Height (mm)	Weight (g)	RD
RA1	48.188±0.036	15.022±0.051	11.589±0.603	0.423±0.021
RA2	48.238±0.014	15.090±0.090	15.860±0.295	0.575±0.012
DA1	48.182±0.054	14.896±0.074	10.465±1.063	0.385±0.038
DB1	48.233±0.036	14.976±0.067	9.929±0.623	0.363±0.022
D1	48.216±0.017	14.880±0.061	9.550±0.427	0.351±0.016
OCT1	48.212±0.048	15.026±0.078	11.244±1.307	0.410±0.046
OCT2	48.185±0.052	15.052±0.046	15.795±0.793	0.575±0.028
OT1	48.193±0.034	14.994±0.055	10.586±0.859	0.387±0.030
OT2	48.164±0.022	15.032±0.104	14.949±0.827	0.546±0.030
BCC1	48.161±0.023	14.690±0.115	7.661±0.536	0.286±0.020
BCC2	48.177±0.019	14.846±0.122	10.078±0.623	0.372±0.021

Table 2 Weight and dimensional measurement results for fabricated samples

Mechanical testing experimentation

The fabricated samples were subjected to quasi-static compressive testing, pendulum impact testing, and drop-weight impact testing. The quasi-static compressive testing was carried out on an Instron 5569A universal testing system. A 5kN load cell was used for the testing, and the strain was calculated from the displacement of the crosshead. Each sample was compressed to 50% of the total strain before the test terminated. Only 1 arbitrarily selected sample from each type of design was tested, which aims to establish the baseline mechanical property knowledge with

the structures. The pendulum impact testing was carried out on a Zwick 5109 pendulum resilience rebound tester following the DIN53512 testing standard. 2 samples of each design were tested. With each sample, 10 automatically controlled pendulum impacts of 0.5J incident energy and 1.98m/s incident velocity were applied through the pendulum hammer of 15mm diameter. As the pendulum impact test utilizes the rebound of the pendulum for the evaluation of the elastic energy dissipation characteristic of the structures, and therefore also serves to provide a comparative basis for the dynamic energy absorption investigation of the structures that involve plastic deformation and fracture damage. The drop-weight impact testing was carried out on an Instron/Dynatup 8250 impact tester. Fig.3 shows the drop-weight impact system setup. The system was equipped with accelerometer (PCM 350B04) and dynamic force transducer (PCM 200C20), which allows for the measurement and calculation of the acceleration, velocity, location and force during the impact. 1 sample from each type of design was subjected to the drop weight impact. Each sample was secured on a solid substrate by double-side tapes and subjected to up to 5 free-drop impact strikes with fixed energy level of 6.17J. For each impact strike, the energy absorption/dissipation window was defined to occur between the initiation of the impact contact and the time when the impactor speed reduced to zero, i.e. the impactor stopped moving downwards, as illustrated in Fig.3b. The total amount of energy absorption (E) during this period was calculated from the force and displacement of each step as:

$$E = \sum_{step1}^{stepn} \left(\frac{F_i + F_{i+1}}{2} \right) x_i \qquad (1)$$

where F_i is the recorded reaction force at step i, and x_i is the corresponding displacement at step i. As the data acquisition rate of both the accelerometer and the force transducer were set at 10.24kHz, each time step corresponds to 9.765625×10^{-5}s.

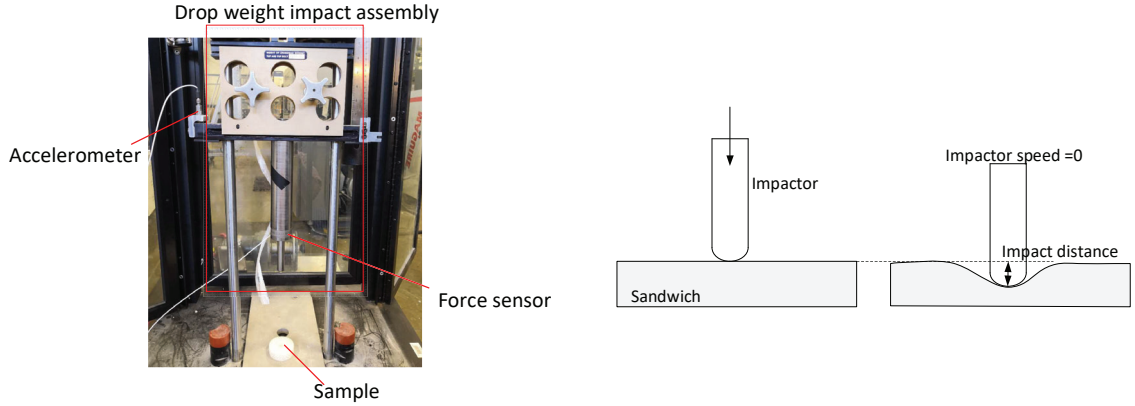

a. Instrumented drop weight testing setup b. calculation of the impact distance

Fig.3 Drop-weight impact testing

Results and discussions

The quasi-static compressive testing stress-strain curves for different types of cellular sandwich structures are shown in Fig.4. All the structures exhibit the typical three-stage cellular structure compression characteristics, including the initial elastic compression stage, the plateau stage, and the final densification stage. On the other hand, it was observed that the elastic stages of all the structures are rather insignificant. Considering the typical low elastic modulus of the TPU materials, it was speculated that the use of crosshead displacement for the evaluation of deformation strain might not be adequately sensitive for this particular study.

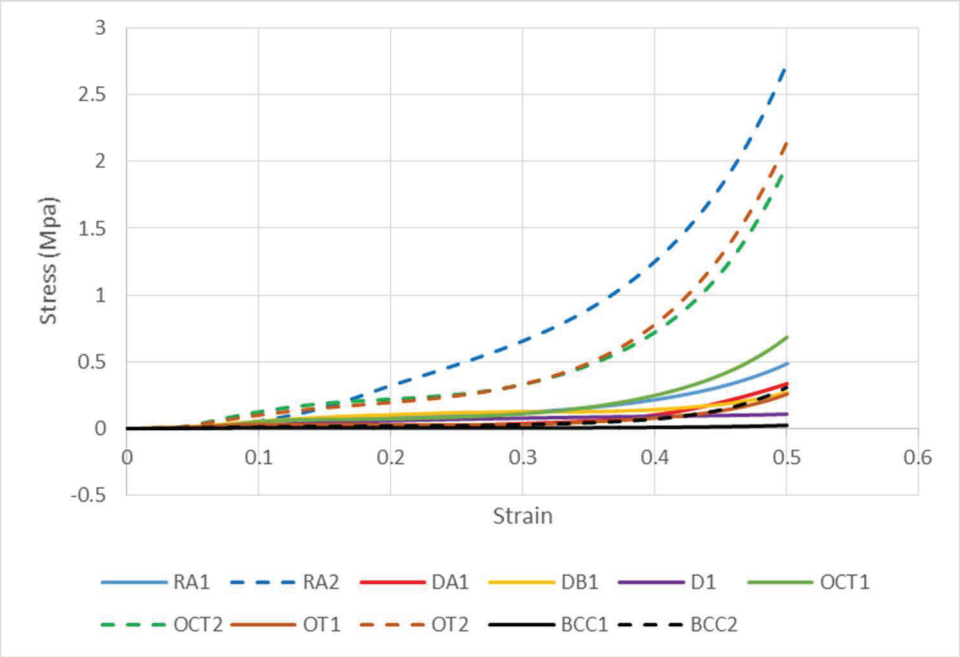

Fig.4 Stress-strain curves of different cellular structures under quasi-static compression

In order to overcome such issue, the stress-strain curve analysis method proposed by Christensen [35] was adopted. The schematics of the treatment is shown in Fig.5. Firstly, the stress-strain curve of a structure was fitted by a 6-order polynomial function, which was then taken to calulation the 1st and 2nd order derivatives for the stress-strain functions. The yield point was identified as the first local minimum of the 2nd derivative of stress-strain functions, as marked out in red arrow in Fig.5c. Utilizing the yield point, the elastic modulus was then calculated by manually selecting the original stress-strain curve segments prior to the yield point and calculate the linear fitting functions. In addition, the total energy absorption of each structure was also calculated from the force-displacement relationships of the compressive testing up to the total strain level of 0.5. After completely unloaded, none of the samples exhibited discernable permanent deformation and visible damage.

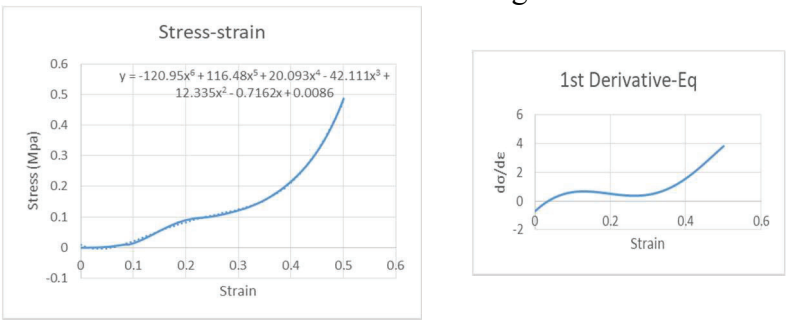

a. Stress-strain curve b. 1st-order derivative c. 2nd-order derivative

Fig.5 Analysis of the quasi-static stress-strain curves

Table 3 shows the elastic modulus, yield strength and energy absorption performance of each types of cellular sandwich structures. Both stretch-dominated designs, the OCT and OT structures, exhibit high mechanical properties at both relative density levels, as well as total energy absorption capabilities. The RA auxetic design also exhibit high mechanical properties and energy absorption capabilities, which appears to be in good agreement with previous studies on PA12

sandwich structures fabricated by laser sintering PBF-AM [36]. Other structures generally exhibit comparatively low mechanical properties as well as energy absorption characteristics. The BCC structure in particular exhibit extremely low performance at low relative density level (BCC1-1), which was also previously observed [36]. It is also worth noting that the BCC structures were among the most easily cleanable structures, as is evident from the relative density results as shown in Table 2. Therefore, it was speculated that the loose powder that were not completely removed from the interior of some of the cellular sandwich samples might contributed to some of the energy absorption capabilities. Fig.6 shows the comparison of energy absorption capabilities among different designs.

Design	Elastic modulus (MPa)	Yield strength (MPa)	Energy absorption (J)
RA1	0.8595	0.0877	1.7760
RA2	3.1828	0.4115	9.5118
DA1	0.2839	0.0590	0.8580
DB1	0.8514	0.0909	1.4567
D1	0.4857	0.0478	0.8138
OCT1	0.9927	0.0611	2.0738
OCT2	2.1019	0.1588	6.0683
OT1	0.5989	0.0294	0.7256
OT2	1.6645	0.1352	6.3644
BCC1	0.0578	0.0041	0.0819
BCC2	0.1631	0.1352	0.6750

Table 3 Quasi-static mechanical properties of different TPU cellular structures

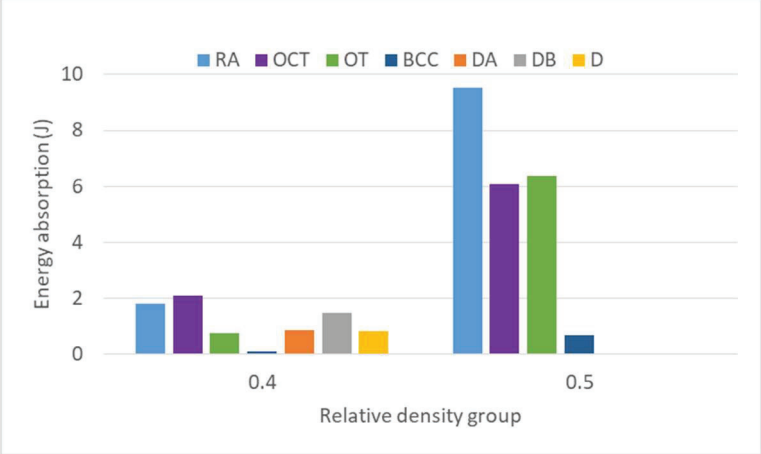

Fig.6 Comparison of quasi-static energy absorption capabilities among different designs

The rebound resilience testing results are summarized in Table 4 and Fig.7. Due to the scheduling limitation with the samples during the rebound resilience testing, the result from RA2 design was unavailable. For the rebound resilience testing, higher rebound percentage indicates less energy dissipation during the elastic deformation of the sample. From Table 7, all the low-relative density variants of each cellular design exhibit higher energy absorption capabilities. The BCC cellular designs appear to exhibit the highest energy absorption capabilities among all the structures. There does not appear to exist a correlation between the rebound resilience and quasi-

static energy absorption. Instead, the overall resilience performance appear to be primarily driven by relative densities of the structures. As shown in Fig.7a, it appears that there exist a linear relationship between the relative density and the rebound resilience across the entire design spectrum. Such behavior appears to suggest that for the elastic rebound energy dissipation performance, the intrinsic material property plays a more dominant role, whereas the cellular topology design might be less significant. However, such speculation should be subjected to further investigation, potentially at broader range of energy levels and impact velocities.

In addition, it was also noted that there exist noticeable energy absorption capability degradation for all the cellular designs, although such trend tend to be smaller with low-relative density variations. As shown in Table 7 and Fig.7b, for all the samples of different cellular designs, the energy absorption capability degradation appear to be most significant at the first 2-3 impact strikes. Afterwards, the degradation appears to be much less obvious. The degradation rate appears to be significantly impacted by the cellular topology design as well, although more design variations are likely needed to verify such hypothesis. Furthermore, one sample (DA1) was arbitrarily selected to undergo further impacts in order to verify the presence of performance degradation. As shown in Fig.7c, the structures continue to exhibit rebound resilience degradation throughout the entire 180-impact strike process. Such behavior was again attributed to the material characteristics of the TPU material used in this study, although no further data is currently available to further investigate such phenomenon.

Design	Rebound %	% different 1st-10th rebound	Avg. % energy absorption
RA1	33.633±1.105	-11.79	66.367
DA1	55.704±4.051	-29.40	44.296
DB1	50.748±1.312	-8.78	49.252
D1	57.154±1.560	-9.58	42.846
OT1	34.478±1.239	-13.22	63.522
OT2	49.108±0.585	-3.78	50.892
OCT1	40.781±1.237	-10.59	59.219
OCT2	61.073±1.861	-10.59	38.927
BCC1	29.267±1.388	-16.67	70.737
BCC2	37.523±1.167	-11.04	62.477

Table 7 Rebound resilience testing results for different cellular sandwich structures

a. Rebound percentage vs. relative densities

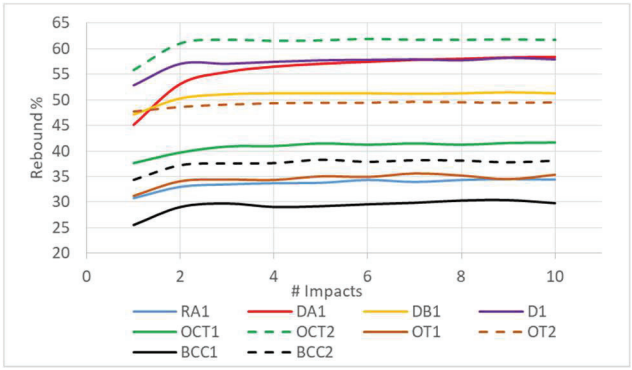

b. Rebound resilience over multiple impacts

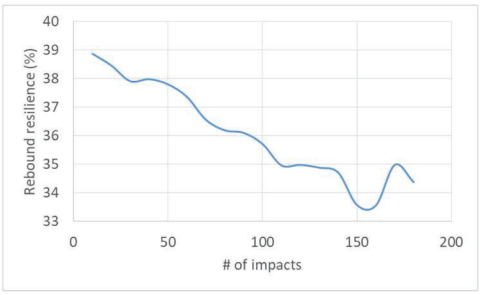

c. Rebound resilience degradation over multiple strikes (DA1)

Fig.7 Rebound resilience characteristics of different designs

The drop-weight impact testing of all the samples resulted in impact strain rates of ~50-65/s. Due to the use of solid substrate as well as the lack of differentiation method between the impacts on the cellular sandwich samples and the impacts on the substrate, the results were subjected to scrutiny during the consequent analysis. Fig.8 shows the accelerations and response forces of the 1st impact for each types of samples. Since no measure was available for the synchronization of drop triggering time at each drop impact, the time stamps for each impact event differ from each other, which can be clearly observed from the different occurrence time of the largest impact peaks in Fig.8, which correspond to the first impacts of each type of structures. In addition, as there is no catching mechanism in the system for secondary impacts from rebounded impactor, multiple impact peaks can be observed for each sample. For the analysis of the energy absorption characteristics, only the first and largest impact event of each structure was further investigated. It is also noted that for the BCC structures the samples at both relative density levels appear to exhibit significantly lower impact deformation resistance, and it was clearly observed during the impact testing that the impactor compressed the BCC sandwich samples to such a degree that the substrate become a significant energy absorber. It was suspected that similar phenomenon was also present with the other designs, although from both the experimental visual observation and the emitted impact sound it was clear that substrate energy absorbing of the other structures are less significant. From the results from quasi-static testing, all the TPU cellular sandwich structures exhibit rather low elastic modulus, which implies that during the initial elastic deformation stages of the drop-weight impact the energy absorption and deceleration processes likely to have only limited contributions to the overall energy absorption behavior. As a result, the effective energy absorbing thickness/distance of the structures is reduced, with the extreme case of the BCC structures where significant amount of energy is absorbed by the substrates.

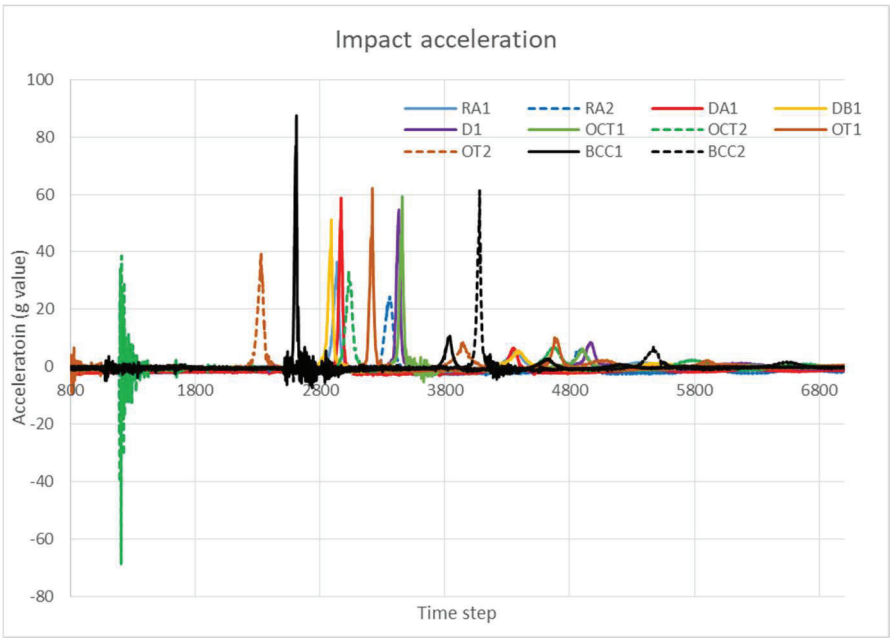

a. Acceleratoin (in g value)

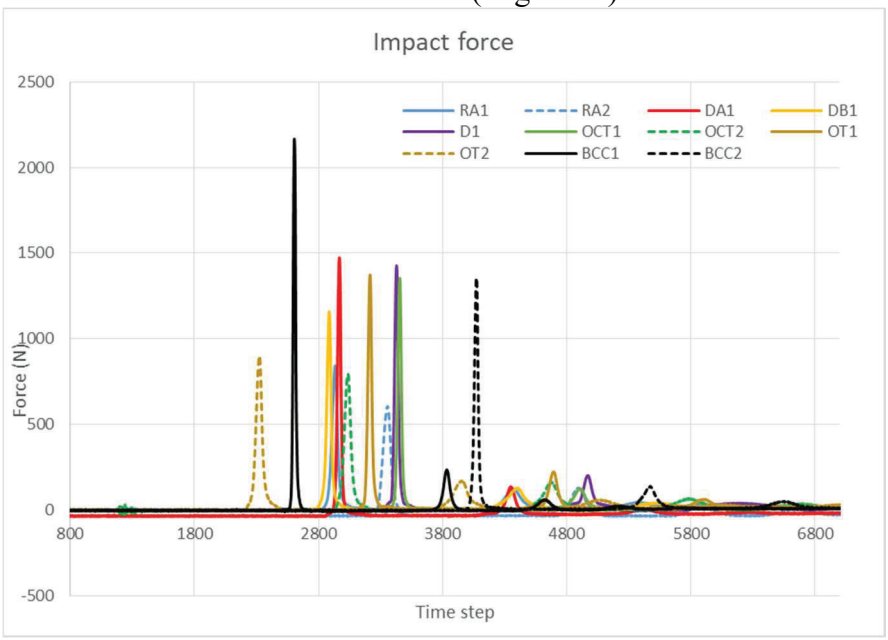

b. Reactive force

Fig.8 Drop-weight impact measurements of different designs

Such notion is further supported by the analysis of the characteristics of the impact characteristics. Fig.9a shows the average impact distances of each types of cellular designs, categorized by their relative density groups. Typically, it can be expected that higher relative densities of cellular structures result in smaller impact distances. However, it can be observed that for most cellular designs the impact distances are around 9-10mm, regardless of the relative density levels. The only exceptions are the low-density BCC (BCC1), which exhibits low impact distance likely due to its ineffective in deformation-induced energy absorption resulted from extremely low elastic modulus, and the RA structures, which consistently exhibit low impact distances of <8mm. It was therefore speculated that for most of the cellular sandwich structures, the thickness of the

structures are inadequate in absorbing the incident energy. The RA structure appears to be the only exception, underlying its exceptional deceleration capability. Fig.9b shows the average energy absorption of different cellular sandwich structures over 5 impact strikes. While it is clear that the high energy absorption of the low-relative density BCC (BCC1) structure was likely attributed to the substrate energy absorption and therefore lacks comparativity, the energy absorption of the other structures should also be subjected to extra scrutiny, mainly due to the likely presence of some substrate energy absorption. With that notion in mind, both stretch-dominated structures, the OCT and OT, exhibit higher energy absorption capabilities compared to the RA structures. Fig.9c shows the average reactive force of different cellular sandwich structures over 5 impact strikes. The significantly higher reactive forces occurred with the BCC structures again suggest that rather rigid substrate-impactor impaction took place. With the other structures, higher relative densities appear to significantly reduce the reaction force levels. This might again be attributed to the reduced substrate-impactor contact with high-relative density designs. The RA designs also exhibit significantly lower reactive force levels. Additionally, it was observed that while the energy absorption and impact distance of each type of cellular structure vary relatively small among the strikes, the reaction forces of the low-relative density cellular designs exhibit obvious increasing trend with increasing strike numbers, as shown in Fig.9d.

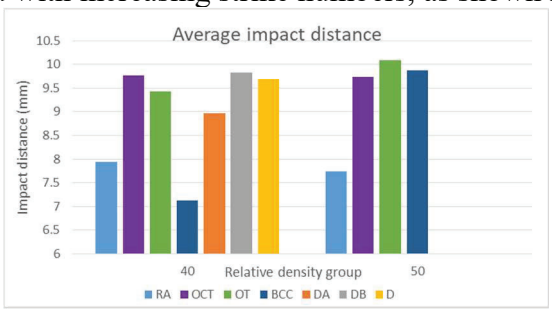

a. Average impact distance

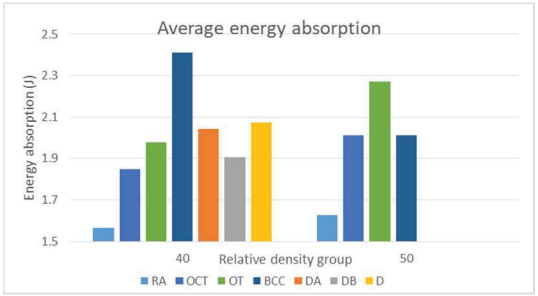

b. Average impact energy absorption

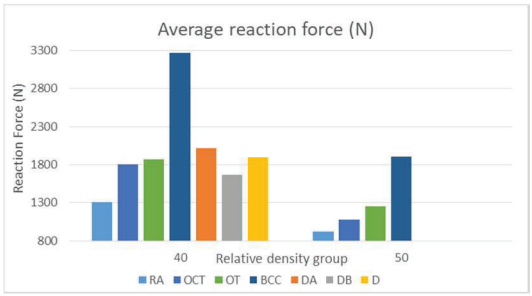

c. Average reaction force

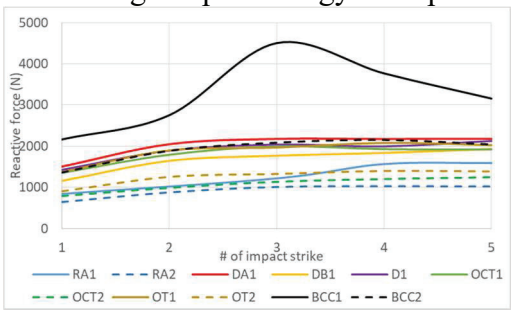

d. Reaction force at each strike

Fig.9 Drop-weight impact characteristics of different TPU cellular sandwich designs

Compared to the results from similar cellular sandwich structures made of PA12 nylon material [51], there exist some discrepancies in the performance of some of the structures. For the RA designs, the structures appear to perform consistently well regardless of the material. On the other hand, the OCT structure appears to exhibit enhanced total energy absorption capabilities when TPU is used as the material, albeit also exhibiting high impact reactive force levels that might be sometime undesirable for protection purpose. Such characteristic might be associated with the fact that the softer TPU material allowed for more local elastic deformation and buckling, which reduced the softening effect that typically occurs with this type of structures when more rigid material is used. However, such speculation requires further investigation. Finally, compared to the quasi-static energy absorption characteristics, a rough correlation can be observed. The three

cellular designs that exhibit the highest quasi-static energy absorption, RA, OCT and OT, also appear to exhibit the most desirable drop-weight impact characteristics, i.e. good compromise between energy absorptions and reactive force levels.

Conclusions

In this study, the dynamic impact energy absorption characteristics of various cellular structure designs made of TPU materials were evaluated. In general, the low elastic modulus and high ductility of the TPU materials introduced significant effect to the overall behaviors of the sandwich structures. Among the different cellular designs, the re-entrant auxetic (RA) design appears to exhibit the most prominent drop-weight energy absorption capabilities. On the other hand, the material enhancement effects from the TPU material appears to be most significant for the stretch-dominated designs, including the octet-truss (OT) and octahedral (OCT) structures. The BCC design appears to exhibit the lowest overall drop-weight energy absorption capabilities. It is hypothesized that the sparsity of the strut arrangement and the low elastic modulus of the BCC structure might be the primary contributing factors. On the other hand, the elastic impact energy absorption of the TPU cellular designs appear to be primarily dependent on the relative densities based on the observations of the current study. Such conclusion contradicts with the general notion about the effect of geometry designs, therefore further investigations is needed.

Acknowledgement

This work is partly inspired and supported by BASF 3D Printing Solutions, Heidelberg, Germany. The authors would like to acknowledge the support of experimentation from Rapid Prototyping Center (RPC) at University of Louisville.

Reference

[1] R. L. Sierakowski. Strain rate behavior of metals and composites. Convergno IGF XIII Cassino 1997, Italy, 1997.
[2] T. Thomas, H. Mahfuz, L. A. Carlsson, K. Kanny, S. Jeelani. Dynamic compression of cellular cores: temperature and strain rate effects. Composite Structures. 58(2002): 505-512.
[3] J. U. Cho, S. J. Hong, S. K. Lee, C. Cho. Impact fracture behavior at the material of aluminum foam. Materials Science and Engineering A. 539(2012): 250-258.
[4] A. Taherkahani, M. Sadighi, A. S. Vanini, M. Z. Mahmoudabadi. An experimental study of high-velocity impact on elastic-plastic crushable polyurethane foams. Aerospace Science and Technology. 50(2016): 245-255.
[5] I. Elnasri, H. Zhao. Impact perforation of sandwich panels with aluminum foam core: a numerical and analytical study. International Journal of Impact Engineering. 96(2016): 50-60.
[6] W. E. Backer, T. C. Togami, J. C. Weydert. Static and dynamic properties of high-density metal honeycomb. International Journal of Impact Engineering. 21(1998), 3: 149-163.
[7] H. Zhao, I. Elnasri, Y. Girard. Perforation of aluminum foam core sandwich panels under impact loading- an experimental study. International Journal of Impact Engineering. 34(2007): 1246-1257.
[8] S. Pattofatto, I. Elnasri, H. Zhao, H. Tsitsiris, F. Hild, Y. Girard. Shock enhancement of cellular structures under impact loading: Part II analysis. Journal of the Mechanics and Physics of Solids. 55(2007): 2672-2686.

[9] L. J. Gibson, M. F. Ashby, Cellular Solids: Structure and Properties, 2nd edition, Cambridge University Press, Cambridge, UK, 1999.
[10] M. F. Ashby, A. Evans, N. A. Fleck, L. J. Gibson, J. W. Hutchinson, H. N. G. Wadley, Metal Foams: A Design Guide, Butterworth-Heinemann, Woburn, MA, USA, 2000.
[11] U. K. Chakravarty. An investigation on the dynamic response of polymeric, metallic, and biomaterial foams. Composite Structures. 92(2010): 2339-2344.
[12] E. Zaretsky, Z. Asaf, E. Ran, F. Aizik. Impact response of high density flexible polyurethane foam. International Journal of Impact Engineering. 39(2012): 1-7.
[13] F. Scarpa, L. G. Ciffo, J. R. Yates. Dynamic properties of high structural integrity auxetic open cell foam. Smart Materials and Structures. 13(2004): 49-56.
[14] A. Beharic, R. R. Egui, L. Yang. Drop-weight impact characteristics of additively manufactured sandwich structures with different cellular designs. Materials and Design. 145(2018): 122-134.
[15] S. Lee, F. Barthelat, J. W. Hutchinson, H. D. Espinosa. Dynamic failure of metallic pyramidal truss core materials – experiments and modeling. International Journal of Plasticity. 22(2006): 2118-2145.
[16] Z. Ozdemir, E. H.-Nava, A. Tyas, J. A. Warren, S. D. Fey, R. Goodall, I. Todd, H. Askes. Energy absorption in lattice structures in dynamics: experiments. International Journal of Impact Engineering. 89(2016): 49-61.
[17] L. Xiao, W. Song, C. Wang, H. Tang, Q. Fan, N. Liu, J. Wang. Mechanical properties of open-cell rhombic dodecahedron titanium alloy lattice structure manufactured using electron beam melting under dynamic loading. International Journal of Impact Engineering. 100(2017): 5-89.
[18] Y. Shen, W. Cantwell, R. Mines, Y. Li. Low-velocity impact performance of lattice structure core based sandwich panels. Journal of Composites Materials. 48(2014), 25: 3153-3167.
[19] J. A. Harris, R. E. Winter, G. J. McShane. Impact response of additively manufactured metallic hybrid lattice materials. International Journal of Impact Engineering. 104(2017): 177-191.
[20] B. J. Ramirez, O. T. Kingstedt, R. Crum, C. Gamez, V. Gupta. Tailoring the rate-sensitivity of low density polyurea foams through cell wall aperture size. Journal of Applied Physics. 121(2017): 225107.
[21] S. R. G. Bates, I. R. Farrow, R. S. Trask. 3D printed polyurethane honeycombs for repeated tailored energy absorption. Materials and Design. 112(2016): 172-183.
[22] S. R. G. Bates, I. R. Farrow, R. S. Trask. Compressive behaviour of 3D printed thermoplastic polyurethane honeycombs with graded densities. Materials and Design. 162(2019): 130-142.
[23] Q. Chen, J. D. Mangadlao, J. Wallat, A. D. Leon, J. K. Pokorski, R. C. Advincula. 3D printing biocompatible polyurethane/poly(lactic acid)/graphene oxide nanocomposites: anisotropic properties. ACS Applied Materials and Interfaces.
[24] M. F. Ashby. The properties of foams and lattices. Philosophical Transactions of The Royal Society A. 364(2006): 15-30.
[25] A. Vigliotti, D. Pasini. Stiffness and strength of tridimensional periodic lattices. Computer Methods in Applied Mechanics and Engineering. 229-232(2012): 27-43.
[26] L. Yang, O. A. Harrysson, H. A. West II, D. R. Cormier, C. Park, K. Peters. Low-energy drop weight performance of cellular sandwich panels. Rapid Prototyping Journal. 21(2015), 4: 433-442.
[27] L. Yang, O. Harrysson, H. West, D. Cormier. Mechanical properties of 3D re-entrant honeycomb auxetic structures realized via additive manufacturing. International Journal of Solids and Structures. 69-70(2015): 475-490.

[28] V. S. Deshpande, N. A. Fleck. Isotropic constitutive models for metallic foams. Journal of the Mechanics and Physics of Solids. 48(2000): 1253-1283.
[29] J. B. Berger, H. N. G. Wadley, R. M. McMeeking. Mechanical metamaterials at the theoretical limit of isotropic elastic stiffness. Nature. 543(2017): 533-537.
[30] R. S. Ayyagari, M. Vural. Multiaxial yield surface of transversely isotropic foams: Part I-modeling. Journal of the Mechanics and Physics of Solids. 74(2015): 49-67.
[31] H. N. G. Wadley. Multifunctional periodic cellular metals. Philosophical Transactions of The Royal Society A. 364(2006): 31-68.
[32] F. Scarpa, P. J. Tomlin. On the transvers shear modulus of negative Poisson's ratio ratio honeycomb structures. Fatigue and Fracture of Engineering Materials and Structures. 23(2000): 717-720.
[33] R. S. Lakes, K. Elms. Indentability of conventional and negative Poisson's ratio foams. Jurnal of Composite Materials. 27(1993): 1193-1202.
[34] A. Bezazi, F. Scarpa. Mechanical behavior of conventional and negative Poisson's ratio thermoplastic polyurethane foams under compressive cyclic loading. International Journal of Fatigue. 29(2007): 922-930.
[35] R. M. Christensen. Observations on the definition of yield stress. Acta Mechanica. 196(2008): 239-244.
[36] A. Beharic, R. R. Egui, L. Yang. Drop-weight impact characteristics of additively manufactured sandwich structures with different cellular designs. Materials and Design. 145(2018): 122-134.